UV Photodissociation of Ethylamine Cation: A Combined Experimental and Theoretical Investigation

Wilson K. Gichuhi,[†] A. M. Mebel,[‡] and Arthur G. Suits*[,†]

Department of Chemistry, Wayne State University, Detroit, Michigan 48202, United States, and Department of Chemistry and Biochemistry, Florida International University, Miami, Florida 33199, United States

Received: August 20, 2010; Revised Manuscript Received: October 21, 2010

Direct current (DC) slice imaging of state-selected ions is combined with high-level ab initio calculations to give insight into reaction pathways, dynamics, and energetics for ethylamine cation photodissociation at 233 nm. These reaction pathways are of interest for understanding the rich chemistry of Titan's ionosphere recently revealed by the Cassini mission. The result for the H-loss product has a bimodal translational energy distribution, indicating two distinct H-loss pathways: these are assigned to triplet $CH_3CH_2NH^+$ product ions and the singlet $CH_3CHNH_2^+$ species. The distribution shows a modest fraction of energy available in translation and is consistent with barrierless dissociation from the ground state. $HCNH^+$ formation is observed as the dominant channel and exhibits a bimodal translational energy distribution with the faster component depicting a significant angular anisotropy. This suggests a direct excited-state decay pathway for this portion of the distribution. We have also observed the $H + H_2$ loss product as a minor secondary dissociation channel, which correlates well with the formation of $CH_2CNH_2^+$ ion with an exit barrier.

Introduction

As it is now well documented, the presence of a thick reducing atmosphere and a cold environment harboring hydrocarbon surface reservoirs makes Saturn's largest moon, Titan, a large-scale planetary laboratory that is ideal for in situ study of prebiotic evolution processes that may parallel those that occurred in our planet 4.5 billion years ago.[1−11] Being the major species in Titan's upper atmosphere, nitrogen (N_2) and methane (CH_4) are ionized by a combination of solar radiation and electron impact ionization induced by Saturn's magnetospheric electrons producing N_2^+, N^+, CH_4^+, CH_3^+, CH_2^+, and CH^+ ionic species, which further convert into higher molecular mass compounds through complicated ion-neutral chemistry.[1−4,7,10−15] Despite being in its infancy, research on Titan's ionospheric chemistry has been a subject of intense scrutiny[7,10,14−16] since the surprising revelation of its rich chemical composition by the ion neutral mass spectrometer (INMS) on board the Cassini spacecraft.[3,13] The INMS data have indicated that the description of Titan's ion chemistry is crucial for our understanding of not only Titan's upper atmosphere, but also the aerosol formation processes in general. Specifically, the INMS data show the presence of a total of 45 different ions in Titan's ionosphere, with $m/z = 28$ as the most abundant ion. Further analysis of the data identified mass 28 principally as $HCNH^+$ ion, consistent with the theoretical models.[3] Several experimental and theoretical models have been devoted to the study of $HCNH^+$ as an important ion in ion-neutral reactions, including those in Titan's ionosphere. These observations have led to recent suggestions that ion−molecule reactions may be much more important in the formation of Titan's dense aerosol haze than previously believed. On the other hand, due to the nature of the difficulty encountered in Earth-based observations of Titan's upper atmosphere and the limited resolution of chemical analysis performed by the space probes, the composition, formation, and growth pathways of these aerosols remain poorly understood.[15]

To date, numerous studies of haze tholins produced in simulated atmospheres exposed to vacuum ultraviolet (VUV) radiation or electrical discharges have been documented.[4,7,14] Motivated by a need for laboratory investigations in support of models of Titan's atmosphere, Zwier and co-workers have undertaken extensive gas-phase fundamental studies on photochemical pathways of small hydrocarbons such as vinylacetylene and diacetylene and their routes to polyaromatic hydrocarbon (PAH) growth in Titan's atmosphere.[17−20] Leone and co-workers have studied many fundamental reactions relevant to Titan's chemistry, including isomer-selective detection of reaction products involved in the formation of larger hydrocarbons such as benzene and other PAH in Titan's atmosphere.[21,22] Although ion imaging methods have offered a rich research opportunity for studying the photodissociation dynamics of state selected ions under collisionless conditions,[23−26] to our knowledge, very few studies have been devoted to the primary photochemistry of ions that are relevant to Titan's atmosphere. The work presented in this Article has been guided by the hypothesis that primary photodissociation of ions under collisionless conditions, in concert with high-level ab initio calculations, can allow us to investigate the formation mechanisms, reaction pathways, and properties of key species detected by Cassini, even if the subject photodissociation per se may not be directly relevant. We will expand on this point in the Discussion.

Studies on the photodissociation of ethylamine (ETA) cation in the ultraviolet (UV) region are rather scarce. As one of the first members of simple alkyl amines, ETA Rydberg states are similar to those of methylamine, but due to the presence of additional carbon atoms, the number of dissociative 3s Rydberg states in ETA is higher.[27,28,33] In a series of classical investigations by Lorquet and Leclerc[27] using quantum mechanical treatments, it was demonstrated that $CH_3CH_2NH_2^+$ ions, in their ground state, dissociate into a CH_3 radical and a $CH_2NH_2^+$ ion when the vibrational energy in the C−C bond exceeds 0.9 eV.

* Corresponding author. E-mail: asuits@chem.wayne.edu.
[†] Wayne State University.
[‡] Florida International University.

10.1021/jp107913p
Published on Web 12/03/2010

Using a time-of-flight mass spectrometer, multiphoton dissociation of ETA cation at 450 and 532 nm was found to yield $m/z = 28$, 30, and 44 as the major peaks with $m/z = 30$ dominating at both wavelengths.[29] No parent ion was observed at 450 nm, while at 532 nm, the $m/z = 44$ and m/z 28 signals were found to increase. Inarguably, because the electronic clouds of α-C atom in the ion shift toward the N atom, no other fragmentation pathway is expected to compete with the β-(C−C) bond, as was also demonstrated by an electron impact ionization study of aliphatic amines.[30] Bodi et al.,[30] in a threshold photoion photoelectron coincidence spectroscopy (TPEPICO) study, reported that the dominant reaction generates $CH_2NH_2^+ + CH_3$ and H-loss product channels, with the H-loss product channel accounting for less than 10%. The onset for H-loss was calculated to be 9.627 eV, 135 meV below the computed onset for the CH_3 loss. The conclusion from this observation was that the H-loss channel was slow, probably as a result of tunneling. In another related study aimed at obtaining an accurate heat of formation of ethylidenimmonium cation ($CH_3CHNH_2^+$), Harvey and Traeger[31] found the H-loss to be the lowest energy fragmentation pathway of EA cation with an appearance energy of 9.61 eV. However, no direct laboratory investigation of ETA cation dissociation in the UV under collisionless conditions in a molecular beam has been reported. In addition, no theoretical investigations have mapped out a detailed potential energy surface with the various primary and secondary reaction pathways, some of which leads to direct observation of product channels that have been detected in Titan's ionosphere.

We have recently reported on the photodissociation of methylamine cation as a potential starting molecule to explore the features of the potential surface that may lead to the formation of species that are relevant to Titan's ionosphere.[16] It is reasonable to envision that, although ETA cation has not been detected in Titan's upper atmosphere, it is yet another excellent starting molecule that can aid in understanding the ion−molecule reactions related to the formation and reactions of the dominant $HCNH^+$ ion and other isomers depicted on its potential energy surface. In this Article, therefore, we present results on ETA cation photodissociation as a second prototypical amine cation with a rich potential surface that has several primary and secondary product channels that can readily be investigated experimentally using our direct current (DC) slice imaging technique via 1 + 1 resonance enhanced multiphoton ionization (REMPI) strategy. To this end, a combined experimental and theoretical investigation on ETA cation dissociation at 233 nm using direct current (DC) slice imaging and high level ab initio calculation, respectively, is reported. These experimental results on the photodissociation of ETA cation are not intended to document the full suite of related photochemical processes in Titan's ionosphere. Nevertheless, within the theoretical realm provided by the high level ab initio calculations, the ion imaging results strive to reveal and explore important aspects and isolate key reaction pathways and phenomena on the potential surface. Although primary photodissociation of the cation is our main goal in this study, our motivation comes from, on one hand, the need to identify important secondary decomposition reaction pathways on the potential surface and, on the other hand, our interest to explore excited-state dynamics such as the $HCNH^+$ formation that is reported in this Article. The implications for the chemistry of $HCNH^+$ formation and haze formation in Titan's atmosphere will also be considered.

Experimental and Computational Details

Experimental Section. Ethylamine cation dissociation was carried out using a velocity map imaging apparatus[32,33] that was optimized for DC slice imaging.[32,34] A pulsed supersonic molecular beam containing ∼1% ethylamine (stated purity >99.0%) seeded in helium was expanded from a pulsed valve into a differentially pumped source chamber at a backing pressure of ∼2 bar. After passing through a 1 mm diameter skimmer that is located 3.8 cm downstream of the pulsed nozzle orifice, the molecular beam entered into an assembly of velocity mapping ion optics consisting of four electrodes. The presence of a second concentrically aligned 2 mm orifice on the high voltage repeller located 7 cm further downstream ensured that the supersonic molecular beam was well collimated. The collimated molecular beam was then perpendicularly crossed by 233 nm light where 1 + 1 resonance enhanced multiphoton ionization (REMPI) of ETA and the subsequent fragmentation of ETA cation took place. The source chamber was maintained at a pressure of 1.0×10^{-5} (beam on), while the main chamber, where ionization and photofragmentation occurred, was maintained at 5.0×10^{-8} Torr.

The wavelength of the laser light employed in this study was produced by frequency doubling of the output of a tunable, narrow-line width (0.07 cm^{-1}) OPO laser system (Spectra-Physics MOPO HF). The MOPO HF was pumped by the third harmonic of a seeded Nd:YAG laser operating at 10 HZ. The vertically polarized laser beam was then focused (20 cm focal length) into the interaction region. The laser polarization was parallel to the detector plane, while the typical output power employed was ∼0.1 mJ/pulse. Wavelength calibration was achieved using a wavemeter (Coherent Wave Master). In the 1 + 1 REMPI scheme, two photons of 233 nm laser light were used to prepare ground-state ETA cation. Absorption of an additional photon from the same laser pulse leads to fragmentation of the state prepared ETA cation. The low laser powers employed in this study ensured that the occurrence of multiphoton dissociation of the cation was minimized or eliminated. The product ions were accelerated through the multilens velocity mapping assembly and impacted onto a dual microchannel plate array of 120 mm diameter, which was coupled to a P-47 phosphor screen. In this study, repeller voltages of 500 V were employed in conjunction with three other lenses in the velocity mapping scheme to stretch the photofragment ion cloud along the time-of-flight axis. The overall flight path from the laser interaction region to the detector was 100 cm. A narrow gate of about 80 ns was used to appropriately sample the central section of the distribution to implement the slicing condition. The resulting ion image was recorded by a CCD camera (Sony XC-ST50, 768 × 494 pixels) in conjunction with the IMACQ Megapixel acquisition program. The IMAN program[35] was used to obtain the total translational energy and angular distributions of the obtained ion images. Calibration of the ion images was achieved by using experimentally obtained images of CO ($v = 0$, $J = 65$) in the photodissociation of OCS at 230 nm under identical conditions.

Theoretical Methods. Molecular geometries and vibrational frequencies of local minima and transition states of $CH_2CH_2NH_2^+$ cation were calculated at the hybrid density functional B3LYP/6-311** level of theory[36,37] using the Gaussian 98 package.[38] Relative energies of various isomers and species on the ground-state potential surface of ETA cation were refined utilizing the coupled cluster CCSD(T) level of theory[39−42] with Dunning's correlation-consistent cc-pVDZ, cc-pVTZ, cc-pVQZ, and cc-pV5Z basis sets[43] and with further extrapolation

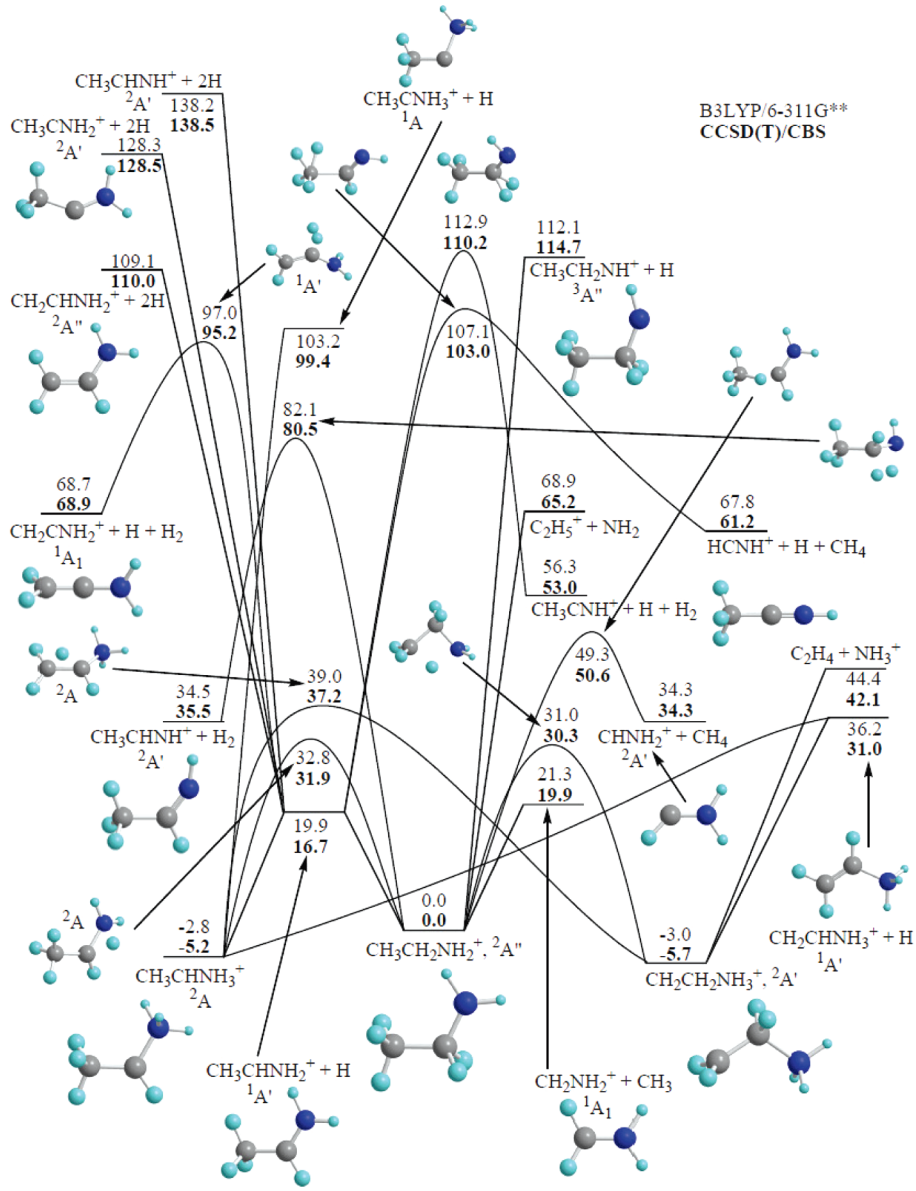

Figure 1. Stationary points on the potential energy surface involved in the photochemistry of the ethylamine cation at 233 nm. The energies were calculated at the B3LYP/6-311G** and CCSD (T)/CBS levels of theory. Energy values are in kcal/mol.

to the complete basis set (CBS) limit.[44] The CCSD(T) calculations were performed using the MOLPRO package.[45] The results of the calculations are summarized in Figure 1, which will guide our presentation and discussion of the experimental results.

Results

Ethylamine exhibits a broad, structured absorption spectrum between 219 and 240 nm, with the most intense peaks appearing at 229.5 and 233.4 nm.[28,46] The lowest lying singlet excited states of ethylamine are expected to be n-3s Rydberg in character.[46,47] One photon excitation of neutral ETA at 233.3 nm is associated with the first member of the amine-wagging vibrational progression.[28] In this case, we suspect that ionization from the Rydberg level is dominated by the diagonal ($v+ = v'$) transition, although we have not confirmed this with photoelectron spectroscopy. The absorption of an additional 233 nm photon by the state-prepared ETA cation leads to subsequent fragmentation, where both primary and secondary product channels are observed. The main channels observed in our experiment are H-loss and formation of $HCNH^+$.

H-Loss Channel. The H-loss ion image and the corresponding total translational energy distribution are presented in Figure 2. The ion image has two components, both of which have an isotropic angular distribution. This ion image gives a bimodal total translational energy distribution upon analysis. The total available energy at 233.3 nm is 123 kcal/mol. In the bimodal translational energy distribution, one component extends to the limit of the available energy for formation of the $CH_3CHNH_2^+$ product but drops off on the low energy side at about 11.5 kcal/mol. A second slow component peaks at very low energy (2.3−4.6 kcal/mol) and drops rapidly at 11 kcal/mol and beyond. On the basis of the potential energy surface profile presented in Figure 1, two H-loss pathways are possible: one is the lowest energy process of all, with a threshold of about 17 kcal/mol; this clearly corresponds to the outer ring in the H-loss image. There is a "hole" in the image for that product, because any of that isomer formed with less than ~20 kcal/mol in translation can undergo secondary decomposition via several pathways and cannot remain bound. The second, very slow isomer must then correspond to the triplet $CH_3CH_2NH^+$ product channel at high

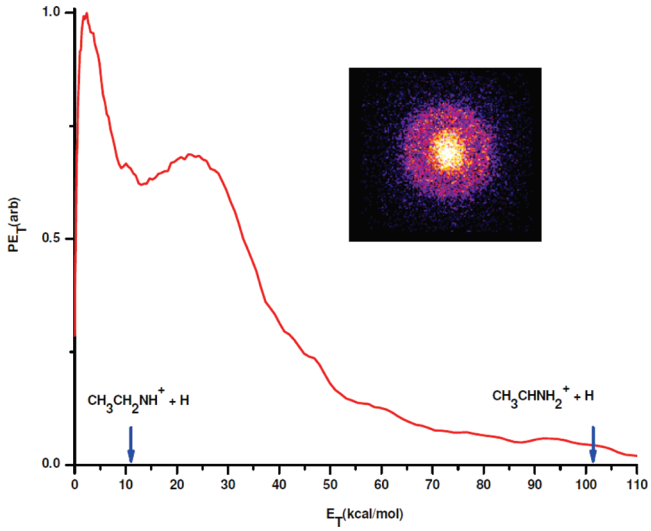

Figure 2. H-loss dc sliced ion image and the associated translational energy distribution for ethylamine cation dissociation at 233 nm.

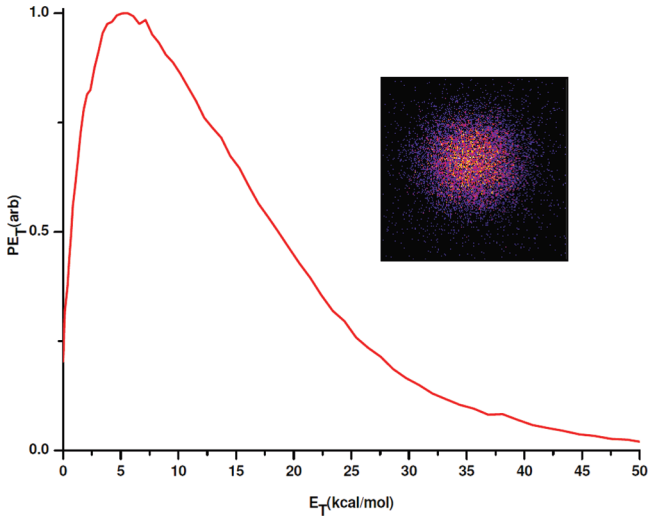

Figure 3. H + H_2 loss image and the associated translational energy distribution for $CH_3CH_2NH_2^+$ cation dissociation at 233.3 nm.

energy. The H-loss translational distribution is consistent with simple bond fission without an exit barrier following an internal excitation to the ground state of the cation.

Formation of *m/z* = 42. Figure 3 shows the DC sliced ion image and the associated translational energy distribution for the formation of $m/z = 42$ product channel. The results show an isotropic angular distribution, which is typical of ground-state statistical dissociation following internal conversion. To understand and identify the dissociation pathway leading to the formation of $m/z = 42$ in our experiment, we turn to the stationary points and reaction pathways of the ground-state cation presented in Figure 1. The $m/z = 42$ product must come from loss of H followed by loss of H_2. As this involves a secondary (three-body) decomposition process, we cannot directly reconstruct the total translational energy from measurement of one fragment only. However, as the initial step is loss of H, we assume negligible translational energy in the $m/z = 43$ product, and obtain the translational energy distribution in Figure 3 by assuming H_2 as the cofragment. Starting from the H-loss product $CH_3CHNH_2^+$, there are two possible routes for the formation of m/z 42. One of these involves H_2 loss over a barrier of 95 kcal/mol, with a reverse barrier of 26 kcal/mol. From our total available energy of 123 kcal/mol, we find that

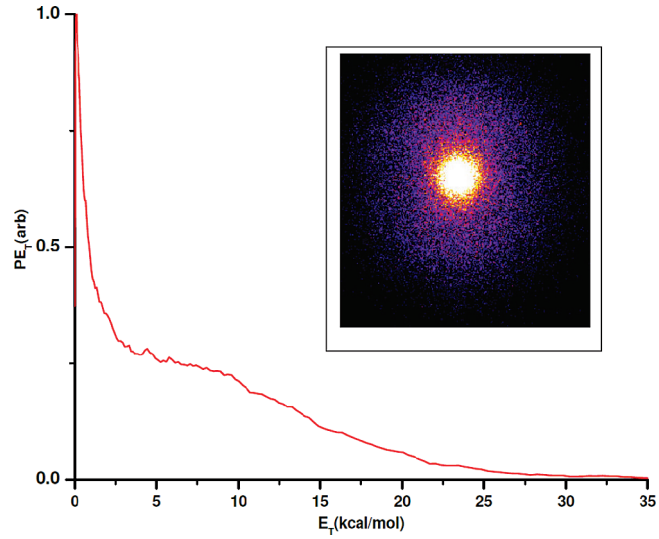

Figure 4. $HCNH^+$ image and the associated translational energy distribution for $CH_3CH_2NH_2^+$ cation dissociation at 233.3 nm.

this channel is open. A perusal of the total translational energy distribution presented in Figure 3 shows the distribution peaking away from zero, with a maximum peak at 5.8 kcal/mol that extends all the way out to 45 kcal/mol, the maximum limit for the formation of $CH_2CNH_2^+$ product channel. On the other hand, the $CH_3CHNH_2^+$ isomer can undergo H_2 loss through a barrier of 110 kcal/mol to form $CH_3CNH^+ + H_2$, a reverse barrier of 57 kcal/mol. Although this channel is about 16 kcal/mol below the $CH_2CNH_2^+ + H + H_2$ channel, the barrier associated with it is 15 kcal/mol higher than that the former; therefore, it is not expected to be competitive. Our DC sliced ion imaging results eliminates this product channel as it would have be expected to show a large fraction of this barrier energy in translation, which we do not observe.

Formation of *m/z* = 28 ($HCNH^+$). We now turn to the results for the formation of the $m/z = 28$ ($HCNH^+$) product channel. Apart from the parent ion ($m/z = 45$) signal, $m/z = 28$ was observed as the most intense peak in our time-of-flight spectrum. It is worth mentioning that the dissociation of $CH_3CH_2NH_2^+$ cation was investigated at wavelengths ranging from 230 to 234 nm, but we only show the results of 233.3 nm as no wavelength dependence was found. At all the investigated wavelengths, $HCNH^+$ formation remained the dominant channel, even at very low laser powers much less than 0.1 mJ. In Figure 4, the DC sliced ion image and the associated translational energy distribution for the formation of $m/z = 28$ are presented. As in the case of $m/z = 42$ discussed above, we neglect the initial recoil in any initial H-loss step and simply assume $m/z = 16$ for the cofragment mass. The ion image has two distinct components, with the faster component showing an appreciable anisotropy. The inner portion of $m/z = 28$ image does not exhibit any anisotropy and peaks at very low energy of 2.3 kcal/mol, dropping off to a limit of 4.2 kcal/mol. The faster component in the $m/z = 28$ image peaks at 4.6 kcal/mol and extends out to 35 kcal/mol. From the potential energy profile presented in Figure 1, $m/z = 28$ can be readily be identified as $HCNH^+$ formation. The $HCNH^+$ can be formed via several pathways, one of which is through the secondary decomposition of $CH_3CHNH_2^+$ to yield $HNCN^+ + H + CH_4$. If we consider the ground-state dissociation of $CH_3CHNH_2^+$, the H_2 loss channel to form $CH_2CNH_2^+ + H + H_2$ is expected to be much more significant than the $HCNH^+ + H + CH_4$ channel. Even at internal energies of 130 and 140 kcal/mol, the RRKM branching

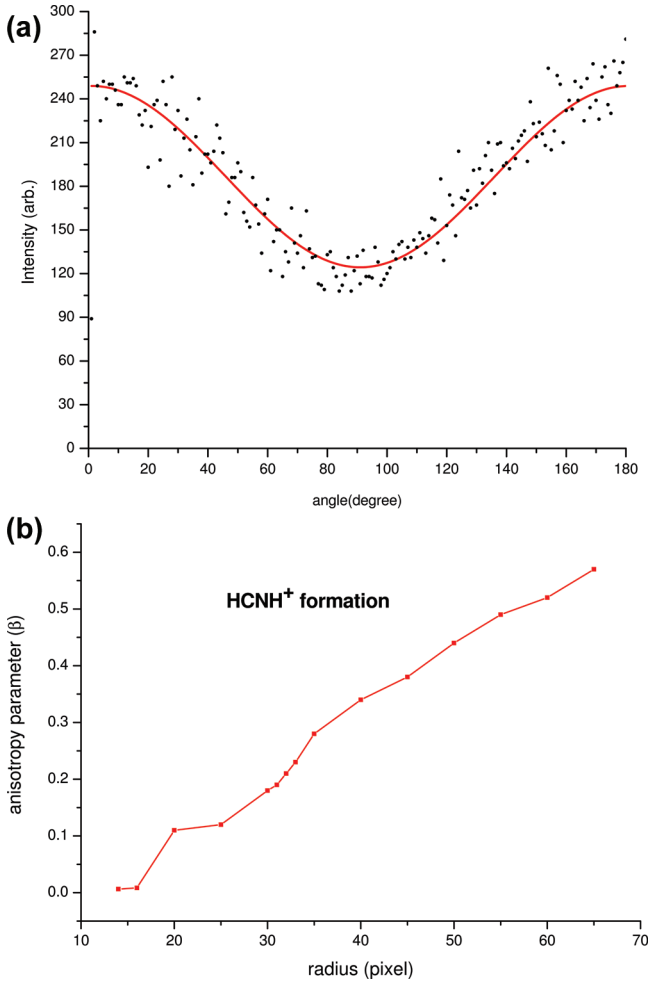

Figure 5. (a) Angular distribution of $HCNH^+$ ion. Solid lines correspond to the best fit with second-order Legendre polynomial term. (b) Anisotropy parameter, β, versus velocity for $HCNH^+$ product channel following 233.3 nm dissociation of ETA cation.

of $HCNH^+ + CH_4$ /$H_2CCNH_2^+ + H_2$ is calculated to be 1:7 and 1.5:6, respectively. The fact that we see appreciable anisotropy in the faster component of the $HCNH^+$ image is an indication that either excited-state dynamics or multiphoton dissociation are involved.

The angular anisotropy parameters describing the angular distributions are obtained by fitting the angular distributions from the ion image to an even-order polynomial expansion:

$$I(\theta)\alpha 1 + \beta_2 P_2(\cos\theta) + \beta_4 P_4(\cos\theta) + \beta_6 P_6(\cos\theta) \quad (1)$$

where θ is the angle between the laser polarization vector and the recoil velocity vector. Figure 5a shows the angular distribution of the faster components of the $HCNH^+$ ion channel. This angular distribution is well fitted using only the second-order Legendre polynomial, giving a β value of 0.57. The measured anisotropies integrated over the entire image from the fast to slow components are presented in Figure 1b. It is clear that the $HCNH^+$ ion image exhibits significant energy dependence in the angular distribution. There is a steady decrease in β with decreasing radius (velocity). A one-photon process can be fully described including only the $P_2(\cos\theta)$ term in eq 1. Because our experiment employs very low laser powers, and given this excellent fit including only the P_2 term, we believe $HCNH^+$ is the product of single photon dissociation and thus probably represents a direct dissociation process from an excited electronic state. These results on $HCNH^+$ formation will be discussed further in the Discussion.

Discussion

The ion imaging results, having identified the H-loss and $HCNH^+$ ion formation as the main primary and secondary dissociation product channels, respectively, can now be examined in light of the high-level ab initio calculations presented in Figure 1. The stationary points and dissociation asymptotes for the ground-state potential energy surface of ETA cation have been calculated at CCSD(T)/CBS and B3LYP/6-311G** levels of theory. It is clearly seen that $CH_3CH_2NH_2^+$ can undergo isomerization through rearrangements to more stable distonic $CH_2CH_2NH_3^+$ and $CH_3CHNH_3^+$ isomers. The barrier heights associated with these rearrangements are 30.3 and 31.9 kcal/mol, and the $CH_2CH_2NH_3^+$ and $CH_3CHNH_3^+$isomers are 5.7 and 5.2 kcal/mol lower in energy than $CH_3CH_2NH_2^+$, respectively. Earlier theoretical work on the potential energy surface of methylamine cation reports a similar isomerization of $CH_3NH_2^+$ to $CH_2NH_3^+$ cation, with an associated barrier height of 7.6 kcal/mol.[48] The lowest primary dissociation channel of $CH_3CH_2NH_2^+$ is H-loss to form $CH_3CHNH_2^+$ at a reaction energy of 16.7 kcal/mol. ETA cation can also lose an H-atom from the NH_2 group to yield a triplet species $CH_3CH_2NH^+ + H$. The triplet $CH_3CH_2NH^+$ cation is located at 98.0 kcal/mol above the singlet $CH_3CHNH_2^+$ product. The other primary channel is the formation of $CH_2NH_2^+ + CH_3$, a process that involves a barrierless cleavage of the β-C−C bond with a reaction energy of 19.9 kcal/mol. CH_4 can also be eliminated through a primary photodissociation process to yield $CHNH_2^+$ cation via a barrier of 50.6 kcal/mol. The reaction energy involved in this process is 34.3 kcal/mol, with the process requiring the breaking of a C−C bond and a significant rearrangement through the $HCNH_2^+$ transition state structure. Another primary decomposition product of ETA cation is located at 65.2 kcal/mol above the parent cation and involves the loss of NH_2 to form the $C_2H_5^+$ cation. Although this channel occurs without an exit barrier, its contribution in the dissociation of ETA cation is not as competitive as the H-loss process that is located 48.5 kcal/mol lower in the potential surface. Within our available energy of 123.3 kcal/mol, $CH_3CH_2NH_2^+$ can also lose H_2 through a barrier height of 80.5 kcal/mol to form CH_3CHNH^+.

We now consider the various secondary dissociation pathways presented in the potential energy profile presented in Figure 1. Once the $CH_3CHNH_2^+$ cation is formed via H-loss, it is expected to undergo secondary decomposition through H_2 loss to form $CH_2CNH_2^+ + H + H_2$. This process occurs with a barrier of 78.5 kcal/mol (above the H-loss product) and involves significant rearrangements. $CH_3CHNH_2^+$ can also undergo barrierless H-loss to yield $CH_2CHNH_2^+$, $CH_3CNH_2^+$, and CH_3CHNH^+ isomers that are located at 93.3, 111.8, and 121.8 kcal/mol above $CH_3CHNH_2^+$, respectively. Among the three H-loss channels from $CH_3CHNH_2^+$, the first is expected to be the most important. The formation of $CH_3CNH^+ + H + H_2$ and $HCNH^+ + H + CH_4$ represents two other pathways in which $CH_3CHNH_2^+$ cation can undergo decomposition. The former channel involving H_2 loss occurs with a barrier of 93.5 kcal/mol and is located at 36.3 kcal/mol above $CH_3CHNH_2^+$, while the latter process involving CH_4 loss takes place with a barrier of 86.3 kcal/mol and is 8.2 kcal/mol higher than the H_2 loss channel.

H-Loss Channel. From our combined experimental and theoretical results on $CH_3CH_2NH_2^+$ cation dissociation at 233.3

nm, one photon dissociation leads to the formation of several primary and secondary product channels in which the primary loss of an H atom to form the singlet $CH_3CHNH_2^+$ ion is the lowest of all. The presence of two components in the ion image and the corresponding bimodal total translational energy distribution presented in Figure 2 is indicative of the formation of triplet and singlet H-loss species that are separated by 98 kcal/mol. Once the singlet $CH_3CHNH_2^+$ cation is formed, it is amenable to further secondary decomposition through H-loss, H_2 loss, and CH_4 loss to form $m/z = 43$, 42, and 28, respectively. Further dissociation of the triplet species on $CH_3CH_2NH^+$ is not energetically allowed. The fast component of the H-loss product channel corresponds to the outer part of the ion image. The presence of a "hole" in this outer ring suggests the occurrence of secondary decomposition of $CH_3CHNH_2^+$ cation via several pathways. The features of the translational energy distribution presented in Figure 2 are consistent with barrierless ground-state statistical dissociation of ETA cation following internal conversion. The first excited states of ETA cation are calculated to be about 2.67 eV above the ground state of the cation.[27] Immediately above the first excited state of ETA cation, there exist numerous other low-lying excited states that are separated by an average energy spacing of about 0.15 eV.[49] At our excitation energy, there are thus many excited electronic states that can facilitate rapid nonradiative electronic relaxation. It is therefore plausible that the absorption of one 233.3 nm photon by ETA cation will lead to subsequent dissociation in the ground state. The lack of anisotropy on the ion image suggests that the lifetime may be long relative to the rotational period of the molecule or that there is a geometry change during the dissociation.

Formation of *m/z* = 42. Turning to the results on the formation of $m/z = 42$ presented in Figure 3, one can clearly see that the translational energy distribution peaks away from zero and falls off at high translational energy limit of 45 kcal/mol. Within our total available energy of 123.3 kcal/mol, it is possible to overcome the barrier leading to the formation of $CH_2CNH_2^+ + H + H_2$. Typically, the ion image associated with dissociation via a barrier should peak away from zero energy as this repulsive energy release is converted to translational energy. The presence of slow $m/z = 42$ products that may result from other multiphoton dissociation processes that are not discussed in this report may contribute to the observation of slow components in the $m/z = 42$ image.

$HCNH^+$ Formation. The $m/z = 28$ image shown in Figure 4 and the corresponding translational distribution are quite interesting. Generally, this kind of bimodal distribution is a clear indication of a photodissociation process resulting from a superposition of two phenomena accompanied by two different translational energy releases, such as in the case of 1,1-difluoroethene dissociation.[50] The slow part of the distribution, represented by the inner ring of the image, has a narrow kinetic energy release peaking near zero and falling off at a very low translational energy release of 16−18 kcal/mol. As mentioned earlier in this Article, one of the central questions raised by our experimental results is the absence of the CH_3 loss channel to yield $CH_2NH_2^+$. One possible explanation would be a rapid decomposition of the initially formed $CH_2NH_2^+$ product ions via H_2 loss to yield $HCNH^+$ product. In an earlier unimolecular decomposition study of $CH_2NH_2^+$, H_2 loss was found to be accompanied by a small fraction of kinetic energy because the $HCNH^+$ formed has bending excitation carrying away the available energy.[51] The average rate constant for the formation of $HCNH^+$ ions from $CH_2NH_2^+$ was calculated to be 6.0×10^4 s^{-1}.[51] If, in our experiment, $CH_2NH_2^+$ loses H_2 to form $HCNH^+$, we expect the inner part of the image to be representative of this process. Indeed, a dissociation pathway involving H_2 loss from $CH_2NH_2^+$ is expected to occur via a barrier of 92.3 kcal/mol as demonstrated in our earlier results on methylamine cation.[16] In principle, secondary decomposition of $CH_2NH_2^+$ does not seem a convincing explanation for the dominance of the slow part of $HCNH^+$ product channel because the process would be too expensive energetically. A major observation to note, however, is the complete disappearance of the angular anisotropy of this inner ring, which strongly suggests that the decay pathways of the slow and faster $HCNH^+$ product channel ion are not the same. We turn now to the faster, anisotropic component of the $HCNH^+$ image in Figure 4. Such anisotropy is unusual, if not unprecedented, in dissociation of polyatomic radical cations, as internal conversion and dissociation from long-lived lower-lying states is the general rule. Instead, these results suggest direct dissociation via an excited state as argued earlier. As shown by the results in Figure 1, the fast $HCHN^+$ could result from secondary decomposition of $CH_3CHNH_2^+$. The image accompanying this process should have a "hole" as this channel has an exit (reverse) barrier of 41.8 kcal/mol. We do not anticipate that this process would be as competitive as the H,H_2 loss channel. At this stage, the participation of excited-state dynamics can be postulated as a likely explanation for the formation of the fast $HCNH^+$ ions because multiphoton dissociation is ruled out by the low laser powers and the good fit to the second-order Legendre polynomial. Unfortunately, Figure 1 can provide no insight into dissociation pathways on the excited state, and such calculations are extremely challenging. We also note we are puzzled by the absence of the $CH_2NH_2^+$ channel in our experiment. Further theoretical studies, including RRKM calculations on the ground state and a full account of the excited-state processes involved, will be helpful to clarify these issues.

We conclude by pointing to a few aspects of this work that may provide additional insight into the chemistry of Titan's ionosphere. Although we do not suggest that photodissociation of methylamine cation is an important reaction to include in Titan's ionospheric models, these results provide detailed theoretical characterization of many important ion−molecule reaction pathways, barriers, and energetics that are confirmed by the experimental results. These include the H-loss and $H + H_2$ loss channels, both of which give closed-shell cations, as well as the dominant $HCNH^+$. These results are thus useful to establish a solid knowledge base on which to build more complete models in the future.

Conclusions

In summary, we report, via a combined experimental and theoretical investigation, results on the dissociation of ETA cation at 233 nm. As the main primary channel observed, the H-loss image has a translational energy distribution with a bimodal structure that correlates well with the formation of singlet $CH_3CHNH_2^+$ and triplet $CH_3CH_2NH^+$ species on the ground-state potential surface of the cation. In addition to H-loss, CH_3 loss to yield $CH_2NH_2^+$ is expected to be an important primary channel according to theoretical results, but we do not observe it in our experiment. $HCNH^+$ is formed as a dominant secondary channel with a bimodal translational energy distribution. The appearance of a significant angular anisotropy on the outer region of the ion image is suggestive of a direct excited-state decay pathway for this fast portion of the distribution, which is a significant portion of the overall yield. $CH_2NH_2^+$

decomposition to $HCNH^+$ occurs at a very high energy so it does not seem a likely explanation for the dominance of this product. The formation of $CH_2CNH_2^+$ is also observed as a minor channel resulting from secondary decomposition of $CH_3CHNH_2^+$.

Acknowledgment. This work was supported by the National Science Foundation under award number CHE-0627854.

References and Notes

(1) Yelle, R. V.; Borggren, N.; de la Haye, V.; Kasprzak, W. T.; Niemann, H. B.; Müller-Wodarg, I.; Waite, J. J. H. *Icarus* **2006**, *182*, 567.
(2) Wilson, E. H.; Atreya, S. K. *J. Geophys. Res.* **2004**, *109*, E06002.
(3) Vuitton, V.; Yelle, R. V.; Lavvas, P. *Philos. Trans. R. Soc.* **2009**, *367*, 729.
(4) Vacher, J. R.; Le Duc, E.; Fitaire, M. *Planet. Space Sci.* **2000**, *48*, 237.
(5) Vacher, J. R.; Le Duc, E.; Fitaire, M. *Planet. Space Sci.* **1997**, *45*, 1407.
(6) Strobel, D. F. *Icarus* **2010**, *208*, 878.
(7) Stavish, L.; Fondren, L. D.; Adams, N. G. *Int. J. Mass Spectrom.* **2009**, *281*, 103.
(8) Sittler, E. C.; Hartle, R. E.; Johnson, R. E.; Cooper, J. F.; Lipatov, A. S.; Bertucci, C.; Coates, A. J.; Szego, K.; Shappirio, M.; Simpson, D. G.; Wahlund, J. E. *Planet. Space Sci.* **2010**, *58*, 327.
(9) Horvath, G.; Aranda-Gonzalvo, Y.; Mason, N. J.; Zahoran, M.; Matejcik, S. *Eur. Phys. J. Appl. Phys.* **2010**, *49*, 13105.
(10) Garnier, P.; Wahlund, J. E.; Rosenqvist, L.; Modolo, R.; Agren, K.; Sergis, N.; Canu, P.; Andre, M.; Gurnett, D. A.; Kurth, W. S.; Krimigis, S. M.; Coates, A.; Dougherty, M.; Waite, J. H. *Ann. Geophys.* **2009**, *27*, 4257.
(11) Cui, J.; Galand, M.; Yelle, R. V.; Wahlund, J. E.; Agren, K.; Waite, J. H.; Dougherty, M. K. *J. Geophys. Res.* **2010**, *115*, A07312.
(12) Zaitsev, V. V.; Shaposhnikov, V. E.; Khodachenko, M. L.; Rucker, H. O.; Panchenko, M. *J. Geophys. Res.* **2010**, *115*, A03212.
(13) Waite, J. H., Jr.; Young, D. T.; Cravens, T. E.; Coates, A. J.; Crary, F. J.; Magee, B.; Westlake, J. *Science* **2007**, *316*, 870.
(14) Imanaka, H.; Smith, M. A. *J. Phys. Chem. A* **2009**, *113*, 11187.
(15) Imanaka, H.; Smith, M. A. *Proc. Natl. Acad. Sci. U.S.A.* **2010**, *107*, 12423.
(16) Singh, P. C.; Shen, L.; Zhou, J.; Schlegel, H. B.; Suits, A. G. *Astrophys. J.* **2010**, *710*, 112.
(17) Cremer, D.; Kraka, E.; Joo, H.; Zwier, T. S. *Phys. Chem. Chem. Phys.* **2006**, *8*, 5304.
(18) Newby, J. J.; Liu, C.-P.; Muller, C. W.; Zwier, T. S. *Phys. Chem. Chem. Phys.* **2009**, *11*, 8316.
(19) Zwier, T. S.; Kraka, E.; Cremer, D. *Phys. Chem. Chem. Phys.* **2006**, *8*, 5317.
(20) Robinson, A. G.; Winter, P. R.; Zwier, T. S. *J. Phys. Chem. A* **2002**, *106*, 5789.
(21) Goulay, F.; Trevitt, A. J.; Meloni, G.; Selby, T. M.; Osborn, D. L.; Taatjes, C. A.; Vereecken, L.; Leone, S. R. *J. Am. Chem. Soc.* **2009**, *131*, 993.
(22) Soorkia, S.; Taatjes, C. A.; Osborn, D. L.; Selby, T. M.; Trevitt, A. J.; Wilson, K. R.; Leone, S. R. *Phys. Chem. Chem. Phys.* **2010**, *12*, 8750.
(23) Nahler, N. H.; Vieuxmaire, O. P. J.; Jones, J. R.; Ashfold, M. N. R.; Eppink, A. T. J. B.; Coriou, A. M.; Parker, D. H. *J. Phys. Chem. A* **2004**, *108*, 8077.
(24) Webb, A. D.; Nahler, N. H.; Ashfold, M. N. R. *J. Phys. Chem. A* **2009**, *113*, 3773.
(25) Singh, P. C.; Shen, L.; Kim, M. H.; Suits, A. G. *Chem. Sci.* **2010**, 552.
(26) Lee, S. K.; Silva, R.; Kim, M. H.; Shen, L.; Suits, A. G. *J. Phys. Chem. A* **2007**, *111*, 6741.
(27) Leclerc, J. C.; Lorquet, J. C. *J. Phys. Chem.* **1967**, *71*, 787.
(28) Hubin-Franskin, M. J.; Delwiche, J.; Giuliani, A.; Ska, M. P.; Motte-Tollet, F.; Walker, I. C.; Mason, N. J.; Gingell, J. M.; Jones, N. C. *J. Chem. Phys.* **2002**, *116*, 9261.
(29) Wei, J.; Zhang, B.; Fang, L.; Zhang, L. D.; Cai, J. Y. *Opt. Commun.* **1998**, *156*, 331.
(30) Bodi, A.; Kercher, J. P.; Bond, C.; Meteesatien, P.; Sztaray, B.; Baer, T. *J. Phys. Chem. A* **2006**, *110*, 13425.
(31) Traeger, J. C.; Harvey, Z. A. *J. Phys. Chem. A* **2006**, *110*, 8542.
(32) Townsend, D.; Minitti, M. P.; Suits, A. G. *Rev. Sci. Instrum.* **2003**, *74*, 2530.
(33) Eppink, A. T. J. B.; Parker, D. H. *Rev. Sci. Instrum.* **1997**, *68*, 3477.
(34) Leskiw, B. D.; Kim, M. H.; Hall, G. E.; Suits, A. G. *Rev. Sci. Instrum.* **2005**, *76*, 104101.
(35) Li, W.; Chambreau, S. D.; Lahankar, S. A.; Suits, A. G. *Rev. Sci. Instrum.* **2005**, *76*, 063106.
(36) Becke, A. D. *J. Phys. Chem.* **1993**, *98*, 5648.
(37) Lee, C.; Yang, W.; Parr, R. G. *Phys. Rev. B* **1988**, *37*, 785.
(38) Frisch, M. J.; Trucks, G. W.; Schlegel, H. B.; Scuseria, G. E.; Robb, M. A.; Cheeseman, J. R.; Zakrzewski, V. G.; Montgomery, J. A.; Stratmann, R. E.; Burant, J. C.; Dapprich, S.; Millam, J. M.; Daniels, R. E.; Kudin, K. N.; Strain, M. C.; Farkas, O.; Tomasi, J.; Barone, V.; Cossi, M.; Cammi, R.; Mennucci, B.; Pomelli, C.; Adamo, C.; Clifford, S.; Ochterski, J.; Petersson, G. A.; Ayala, P. Y.; Cui, Q.; Morokuma, K.; Salvador, P.; Dannenberg, J. J.; Malick, D. K.; Rabuck, A. D.; Raghavachari, K.; Foresman, J. B.; Cioslowski, J.; Ortiz, J. V.; Baboul, A. G.; Stefanov, B. B.; Liu, G.; Liashenko, A.; Piskorz, P.; Komaromi, I.; Gomperts, R.; Martin, R. L.; Fox, D. J.; Keith, T.; Al-Laham, M. A.; Peng, C. Y.; Nanayakkara, A.; Challacombe, M.; Gill, P. M. W.; Johnson, B.; Chen, W.; Wong, M. W.; Andres, J. L.; Gonzalez, C.; Head-Gordon, M.; Replogle, E. S.; Pople, J. A. *Gaussian 98*, revision A.11; Gaussian, Inc.: Pittsburgh, PA, 2001.
(39) Scuseria, G. E.; Janssen, C. L., III; H, F. S. *J. Chem. Phys.* **1988**, *89*, 7382.
(40) Scuseria, G. E., III; H, F. S. *J. Chem. Phys.* **1989**, *90*, 3700.
(41) Pople, J. A.; Head-Gordon, M.; Raghavachari, K. *J. Chem. Phys.* **1987**, *87*, 5968.
(42) III, G. D. P.; Bartlett, R. J. *J. Chem. Phys.* **1982**, *76*, 1910.
(43) Thom, H.; Dunning, J. *J. Chem. Phys.* **1989**, *90*, 1007.
(44) Peterson, K. A.; Dunning, T. H. *J. Phys. Chem.* **1995**, *99*, 3898.
(45) MOLPRO, a package of ab initio programs designed by: Werner, H.-J. a. K., P. J.; version 2002.1. Amos, R. D.; Bernhardsson, A.; Berning, A.; Celani, P.; Cooper, D. L.; Deegan, M. J. O.; Dobbyn, A. J.; Eckert, F.; Hampel, C.; Hetzer, G.; Knowles, P. J.; Korona, T.; Lindh, R.; Lloyd, A. W.; McNicholas, S. J.; Manby, F. R.; Meyer, W.; Mura, M. E.; Nicklass, A.; Palmieri, P.; Pitzer, R.; Rauhut, G.; Schutz, M.; Schumann, U.; Stoll, H.; Stone, A. J.; Tarroni, R.; Thorsteinsson, T.; Werner, H.-J.
(46) Streibel, T.; Hafner, K.; Mühlberger, F.; Adam, T.; Zimmermann, R. *Appl. Spectrosc.* **2006**, *60*, 72.
(47) Andrews, S. R.; Parry, D. E.; Harris, F. M. *J. Mass Spectrom.* **1995**, *30*, 1694.
(48) Bouma, W. J.; Dawes, J. M.; Radom, L. *Org. Mass Spectrom.* **1983**, *18*, 12.
(49) Krier, C.; Lorquet, J. C.; Berlingin, A. *Org. Mass Spectrom.* **1974**, *8*, 387.
(50) Gridelet, E.; Dehareng, D.; Locht, R.; Lorquet, A. J.; Lorquet, J. C.; Leyh, B. *J. Phys. Chem. A* **2005**, *109*, 8225.
(51) Choi, T. H.; Park, S. T.; Kim, M. S. *J. Chem. Phys.* **2001**, *114*, 6051.

JP107913P